Reinforced conductive polyester based on itaconic acids, glycerol and Polypyrrole for tissue engineering applications

Pejman Ghaffari-Bohlouli[1,2], Najmeh Najmoddin[3], Vahabodin Goodarzi[1*], Wei-Hsin Chen[4,5,6] , Amin Shavandi[2]

[1] Applied Biotechnology Research Center, Baqiyatallah University of Medical Sciences, Tehran, Iran

[2] Université libre de Bruxelles (ULB), École polytechnique de Bruxelles-BioMatter unit, Avenue F.D. Roosevelt, 50 - CP 165/61, 1050 Brussels, Belgium

[3] Department of Biomedical Engineering, Science and Research Branch, Islamic Azad University, Tehran, Iran

[4] Department of Aeronautics and Astronautics, National Cheng Kung University, Tainan 701, Taiwan

[5] Research Center for Smart Sustainable Circular Economy, Tunghai University, Taichung 407, Taiwan

[6] Department of Mechanical Engineering, National Chin-Yi University of Technology, Taichung 411, Taiwan

Corresponding authors:

Vahabodin Goodarzi, v.goodarzi@hotmail.com, and v.goodarzi@bmsu.ac.ir

Abstract

Modified chemically crosslinked polyesters as soft and electroconductive materials for tissue engineering applications have gained notable attention. In this work, electroconductivity, thermal stability, and mechanical properties of synthesized Poly (glycerol-sebacate-itaconic) (PGSIT) by the solvent-free method was improved by incorporating polypyrrole (PPy) and clay within the PGSIT matrix. Hydrogen bonds between PGSIT and PPy lead to a homogeneous dispersion of clay and PPy within the PGSIT matrix. The evaluations indicated that PPy and clay could raise the conductivity of PGSIT to 1.4×10^{-4} S/cm, Young's modulus to 0.9 MPa, tensile strain to 0.91 MPa, and improve the thermal stability and hydrophilicity of the matrix. Moreovere, the toxicity of the developed matrix was studied by MTT assay. According to the results, the PGSIT-PPy-clay composite might be used as a electroconductive bio-elastomer in tissue engineering applications.

Keywords: Polyester; Polypyrrole; clay; Electroconductive; Tissue engineering

1. Introduction

In recent years, synthetic implants and tissue transplants have been replaced with tissue engineering procedure that creates 3D scaffolds from degradable porous biomaterials and combines them with biological cells or molecules [1]. These scaffolds require biomaterials that are mechanically and structurally compatible with the target tissue while facilitating tissue healing through molecular interactions [2][3]. Generally, synthetic polymers offer more flexible properties than natural materials, making them very desirable as constituent materials for scaffold manufacturing. They have been widely applied in human biomedical applications such as tissue engineering [4], drug delivery systems, and wound healing, in the form of shape memory polymers [2], hydrogels, nanoparticles, and nanofibers [5].

Aliphatic polyesters, as a derivative of synthetic polymers, could provide a wide range of required properties for biomedical applications by modifying reaction and processing conditions and also the nature of initial chemicals [6]. Designing and developing elastic materials for muscles, cardiac, and skin are crucial since these materials require adequate shape-recovery to mimic tissue elasticity without rupture and irritating surrounding tissues [7]. However, polyesters such as poly (lactic Acid) (PLA)[6,8–10], Poly (caprolactone) (PCL)[11], and Poly (lactic-co-glycolic Acid) (PLGA)[12] have been used in a variety of biomedical applications; these polymers suffer from rigidity and poor deformation ability for soft tissues. The use of new rubber-like aliphatic polyesters, which are biocompatible and elastic, with a straightforward synthesis method, and resorbable by-products such as Poly (xylitol dicarboxylates) (PXD)[13], Poly (glycerol sebacate) (PGS)[14,15], Poly (glycerol succinic) (PGSu)[16] and other solvent-free produced polyesters have been widely reported. Poly (glycerol-itaconic Acid) (PGI) is a unique bio-resorbable polyester synthesized through the melt condensation of itaconic Acid and glycerol, with promising results for utilization as coatings, adhesives, and phase change materials [17,18]. Constituents of PGI are bioresorbable. Itaconic Acid is a biomass-derived unsaturated acid produced industrially by fermentation of carbohydrates and glycerol which is a building block of tri-glyceride, a typical lipid in the human body. PGI follows a two-step polymerization; 1. synthesizing meltable and wax-like pre-polymer, and 2. Crosslinking the pre-polymer via high temperature and vacuum. Copolymerization of the pre-polymers of PGI with Poly (ethylene glycol) (PEG) and ammonium

polyphosphate (APP) could modify the properties of the synthesized product and extend its applications in the field of stable flame retardant and phase change materials [18].

Conductive biomaterials, such as polypyrrole (PPy), polythiophene, polyaniline, polyphenylene, and polyacetylene, could transfer cell signals and respond intelligently to electrical domains under physiological conditions by supplying π-bonding [19,20]. So far, many applications of this type of conductive polymer have been demonstrated and approved, including piezoresistive composites[21][22], energy storage supercapacitors[23][24], electromagnetic shielding[25], and water treatment[26][27]. In the field of electroactive scaffolds for tissue regeneration, PPy plays a critical role among conductive polymers. Although PPy is biocompatible and stable in the environment [28], it has a brittle structure with low hydrophilicity [20,28]. PPy has been blended within the rubber-like polymer matrix to take advantage of its mechanical properties and improve the conductivity of the host bio-elastomer matrix [28]. Fantino et al. [29] combined PPy within the 3D printed Poly (ethylene glycol) diacrylate hydrogels, which diminished the template's resistivity by more than one order of magnitude. Similarly, a semi-conductor self-heal hydrogel has been synthesized by Sander et al. [30], which demonstrated an electrical conductivity of higher than 10^{-5} S/cm. Moreover, adding PGS to the reaction media of collagen and PPy improved the system's electrical conductivity and cell adhesion [31].

The present work aims to incorporate PPy into itaconic acid-based polyesters as a conductive composite to develop electroactive biomaterials for tissue regeneration. In this work, a series of newly electroactive and flexible Poly (glycerol-sebacate-itaconic) (PGSIT)/PPy was synthesized, and the mechanical properties of the synthesized polyester were improved with clay. The synthesized composites were studied by Fourier transform infrared (FT-IR) spectroscopy, X-ray diffraction (XRD), and field-emission scanning electron microscopy (FE-SEM). A more in-depth evaluation of the performance in terms of mechanical and thermodegradation as well as electrical conductivity was accomplished. Furthermore, the biocompatibility of the synthesized composite was studied by evaluating the viability of the L929 cells in extracted media from the synthesized composite.

2. Experimental details

2.1. Materials

Glycerol (>99%), ferric chloride ($FeCl_3$), stannous octoate ($Sn(Oct)_2$), and hydrochloric acid (HCl, 1 mol/l) were supplied by Merck. Clay (Cloisite 30B grade) was purchased from Saturn. Sebacic Acid (99%), itaconic Acid (>99%), pyrrole (reagent grade, 98%), 1,4-Dioxane (anhydrous, 99.8%), 4-methoxyphenol (MEHQ), p-toluenesulfonic acid monohydrate, dibutyltin dilaurate (DBTL), and hexamethylene diisocyanate (HDI, 98%) were all procured from Sigma-Aldrich. All raw materials were of analytical grade and used in their original condition.

2.2. Sample preparation

2.2.1. Synthesis of PGSIT pre-polymers

PGSIT pre-polymer was synthesized following the procedure described in the literature [32–34]. Briefly, glycerol , sebacic Acid, and itaconic Acid (I.A.) in 1:0.5:0.5 molar ratios were reacted for 2 h in a two-necked flask under the nitrogen flow at 140 °C in an oil bath. To complete the pre-polymerization procedure, the specific amount of p-toluenesulfonic acid monohydrate (0.5% mol proportional to I.A.) and MEHQ (0.5 wt.% per total weight) was added to the reaction flask as the catalyst for pre-polymerization and an inhibitor for the radical polymerization, respectively. Afterward, DBTL (0.5 wt.% per total weight) was added drop-wise to the mixture to catalyze the polycondensation. The reactants were then allowed to maintain at 140 °C for 2 h in vacuum conditions to obtain the PGSIT pre-polymers. The synthesis mechanism is depicted in Fig.1a.

2.2.2. Synthesis of crosslinked PGSIT/PPy/clay composites

The PPy was prepared following the synthesis method reported by Golbaten-Mofrad et al. [35]. 6 mmol of pyrrole and doping agent (HCl, 1 mL) was added to 50 mL of deionized (DI) water and stirred for 30 min to complete the doping process. Subsequently, 0.025 mmol of $FeCl_3$ as an oxidant was combined with the prepared solution to initiate pyrrole polymerization. The polymerization was continued for 48 h and stirred at 150 rpm. The synthesized PPy was rinsed with water until it attained pH 6 and then dried and purified in an oven for one day. The PPy powder was mixed with synthesized PGSIT pre-polymer (3% w/w) at 140 °C and stirred for 24 h.

The PGSIT/PPy pre-polymer mixture was dissolved into 10 mL of a 1,4-Dioxane solution containing 1 gr of HDI and 3 wt.% of clay. The resultant solution was mixed with three drops of $Sn(Oct)_2$ as a catalyst and agitated at ambient conditions for a day. The mixture was cast in the PTFE mold and maintained for 48 h at room temperature to dry and obtain fully crosslinked films. The composition of the synthesized samples is listed in Table 1.

Table 1: The constituents of fabricated biomaterials

sample	PGSIT pre-polymer in solution (g/mL)	clay content (wt.%)	PPy content (wt.%)
PGSIT	0.2	0	0
PGSIT-clay	0.2	3	0
PGSIT-PPy	0.2	0	3
PGSIT-PPy-clay	0.2	3	3

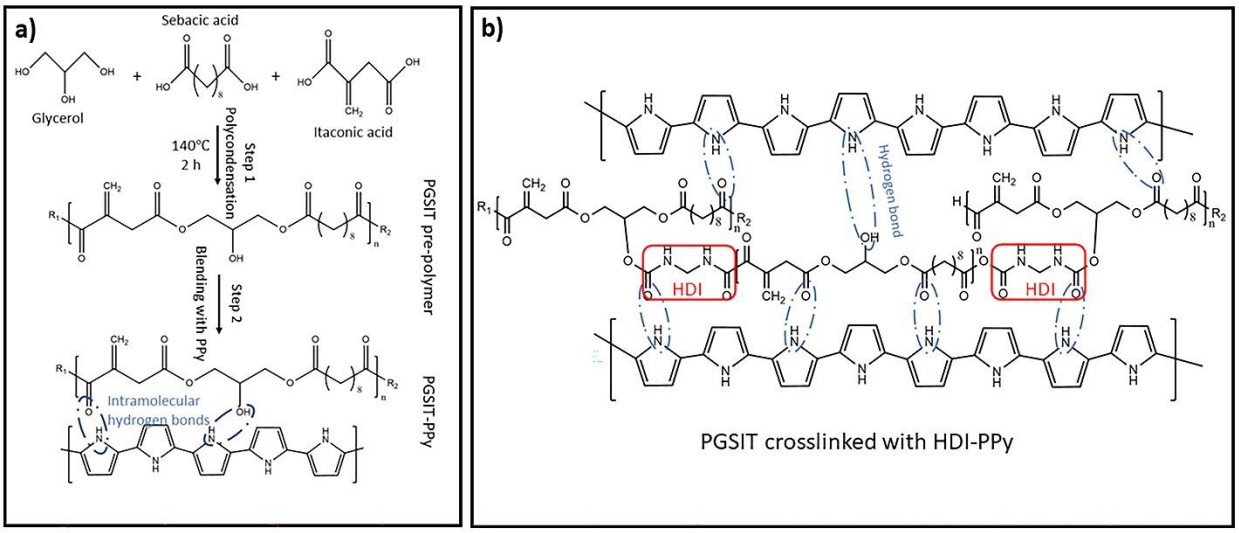

Fig1: (a) The chemical structure of PGSIT and PGSIT-PPy and their possible interactions, and **(b)** the chemical structure of PGSIT crosslinked with HDI containing PPy and the possible intramolecular hydrogen bonds between them.

2.3 Characterization

2.3.1. Fourier Transform Infrared Spectroscopy (FT-IR).

The I.R. spectra of specimens were collected using an FT-IR spectrometer (Thermo Nicolet Nexus 470FT-IRESP) equipped with an ATR module. The absorbance spectra were recorded over the wavenumber range of 600-4000 $cm^{-1,}$ and each sample was subjected to an average of 64 scans at a resolution of 4 cm^{-1}.

2.3.2. X-ray Diffraction (XRD)

The XRD data of the samples were taken using the Ultima IV diffractometer (Rigaku, Japan) with Cu Kα radiation (λ = 1.5418 A˚) operating at a generator voltage of 40 kV and a current of 30 mA. The scan was carried out at an ambient temperature in the 2Θ range of 1° to 50°.

2.3.3. Field emission-scanning electron microscopy (FE-SEM)

The clay's structural morphology, interaction, and dispersion in the polymer matrix were evaluated using the FE-SEM instrument (Mira3, Tescan, Czech Republic, Razi Metallurgical Research Center) with an operating voltage of 15 kV. The samples were broken in half after soaking them in liquid nitrogen. The cross-section of samples was mounted on aluminum stubs with copper adhesive tape. Afterward, each sample was gold-coated by a sputter coater (Emitech K450X). Energy-dispersive spectroscopy (EDS) was applied to identify the microscale elemental distribution.

2.3.4 Surface hydration ability

The surface hydration behavior of the composites was determined by dynamic water contact angle measurement. The timer began when a droplet of DI water detached from the needle and made contact with the sample's surface. Images from various wetting time intervals (0, 30, 60, and 90 s) were acquired using the Dino-lite AM3111 digital microscope, and the contact angle was computed using ImageJ software [36].

2.3.5 Electrical conductivity testing

The electrical parameters of the specimens were assessed using a four-point probe apparatus (FPP-SN-554, Sanat Nama Javan Co, Iran). The experiment was accomplished at room temperature, and the mean value of three replicate tests was reported. In accordance with a method previously mentioned [35,37,38], the equation (1) was used to measure the electrical conductivity of a thin layer of material whose thickness (t, m) is less than the probe spacing (t, m) ($t/S << 5$).

$$\sigma = \frac{\ln 2}{\pi t} \times \frac{I}{V} \qquad Eq\ [1]$$

Where the sample's electrical conductivity (S/cm), current intensity (mA), and voltage (mV) are referred to as σ, I, and V, respectively.

2.3.6 Thermal degradation

Thermal gravimetric analysis (TGA) was performed to evaluate the influence of each component (clay and PPy) on the thermal degradation of the final composite. The test was conducted on the Pyris Diamond Series TG/DTA (Perkin Elmer, USA) instrument in the temperature range of 38-700 °C. The specimens were scanned at a heating rate of 10 °C/min and under an inert nitrogen flow [14].

2.3.7 Mechanical properties

The mechanical performance of the prepared biomaterials was studied by the SANTAM STM-20 testing machine fitted with a load cell of 100 N. Before mechanical testing, the film samples were subjected to hydrated conditions (24 h immersion in PBS at 37 °C). The test was performed for each sample (n = 5, 20 mm × 10 mm × 1 mm) at a constant strain speed of 50 mm/min. The ultimate tensile strength (UTS) and elongation (El.) were calculated from the resulting stress-strain curves, and the initial linear slope was utilized to determine Young's modulus (Y.M.)[16].

2.3.8 *In-vitro* cell biocompatibility

To investigate the sample's cytotoxicity and evaluate the cell growth and proliferation, the samples were first soaked in 70% alcohol for 10 min washed with DI water, and exposed to U.V. radiation for 45 min. In accordance with ISO 10993-5, the extraction method was carried out, during which 1 mL of Dulbecco's Modified Eagle's Medium (DMEM) was added to each sterile sample for every 3 cm^2 of the surface. Following the 3 and 7-day periods, the extract medium was separated and applied to cells. Additionally, DMEM was considered as a control medium. A 96-well cell culture plate was filled with 1×10^4 cells and 100 μL of culture medium to determine the

cell reproduction rate. The cell-contained plate was then placed in an incubator at 37 °C for a day to allow the cells to adhere. After reaching the favorable cells attachment, a portion of the medium was removed from the cells, and 90 µL of each sample's extract was added to each culture well along with 10 µL of fetal bovine serum (FBS). Following this, the cells were placed in contact with these extracts for a period of 24 h. After removing the culture medium, 100 µL of MTT at 0.5 mg/ml was transferred into each well and incubated for 4 h. Subsequently, purple crystals were dissolved with isopropanol once the solution was collected from the cells. For better dissolution, the plate was shaken for 15 min. An ELx808 microplate reader (BioTek) with an optical wavelength of 570 nm was utilized to quantify the concentration of formazan in the isopropanol solution. The culture well with a higher number of cells produces a higher optical density (O.D.) than the culture well with a lower number of cells. Based on equation (2), the culture well with higher amounts of cells was determined and compared to the control sample.

$$\text{Toxicity} = \left(1 - \frac{\text{mean O.D.of the sample}}{\text{mean O.D.of control}}\right) \times 100 \qquad \text{Viability \%} = 100 - \text{Toxicity \%} \qquad Eq\ [2]$$

Scanning electron microscopy at a 10 kV acceleration voltage was used to detect cell adhesion and proliferation on the sample's surface. To investigate the cell adhesion morphology, in a 24-well plate, sterilized samples were inserted into each well individually. Each well received a total of 20000 cells (100 µL), which were then incubated for 4-5 h. After the adherence of cells, a specific portion of the culture medium including 10% FBS was transferred to each well. To fix cells, 3.5% glutaraldehyde was employed after the removal of the culture medium at 1, 3, and 7 days. The fixative agent was spread over the samples and stored in the refrigerator for 2 h, followed by the removal of the fixative. The specimens were washed first with DI water and then with ascending concentrations of ethanol (20, 40, 60, 80, and 96%).

3. Results and discussion

3.1. Chemical and microstructural identification

The functional groups of synthesized PGSIT composites and initial chemicals were characterized by FTIR and compared to authenticate the successful synthesis. As depicted in Fig.2a, the following characteristic PGSIT bands were observed in the 3500-800 cm^{-1} range: C=O

stretching of carbonyl groups at 1720 cm^{-1} [14]; asymmetric and symmetric stretching of CH_2 of alkane at 2920 cm^{-1} and 2860 $cm^{-1,}$ respectively [39]; CH_2 bending at 1460 cm^{-1} [40]; and $C=CH_2$ stretching of itaconic Acid at 1640 and 815 cm^{-1} [17]. The crosslinking reaction of PGSIT-based pre-polymers with HDI led to the formation of urethane linkages confirmed by the appearance of three amide absorption peaks at 1650 cm^{-1} (amide I), 1530 cm^{-1} (amide II), and 1240 cm^{-1} (amide III) [35]. For all crosslinked samples, the broad peak in the wavelength of 3480-3240 cm^{-1} was attributed to the O-H and N-H stretching [41,42]. In the case of the PPy-contained composites, the PPy distinct peaks were overlapped by PGSIT peaks. Fig.2b illustrates the peaks related to signature bands of PPy. The prominent peaks are located at 1311 cm^{-1} (C-N stretching) [43], two peaks at 1556 and 1482 cm^{-1} (C=C stretching) [44], 1038 cm^{-1} (N– H in-plane bending), and 1159 cm^{-1} (C– H in-plane deformation) [35]. Moreover, the out-of-plane deformation of C-H bonds was identified by two peaks at 960 and 920 cm^{-1} [35]. Regarding the clay particles (Fig.2a), typical characteristic peaks were found at 3630 cm^{-1} (-OH stretching), 2860 and 2920 cm^{-1} (-CH stretching from 30B-modifier), and 1020 cm^{-1} (Si-O stretching) [45]. Besides, three types of -O.H. deformation peaks related to Al, 2Al-Mg, and Si-O at 914, 837, and 792 cm^{-1} were detected, respectively, and all of which were in accordance with those declared in the literature [45]. However, in the case of composites, no significant change in band position or intensity was observed in their spectra.

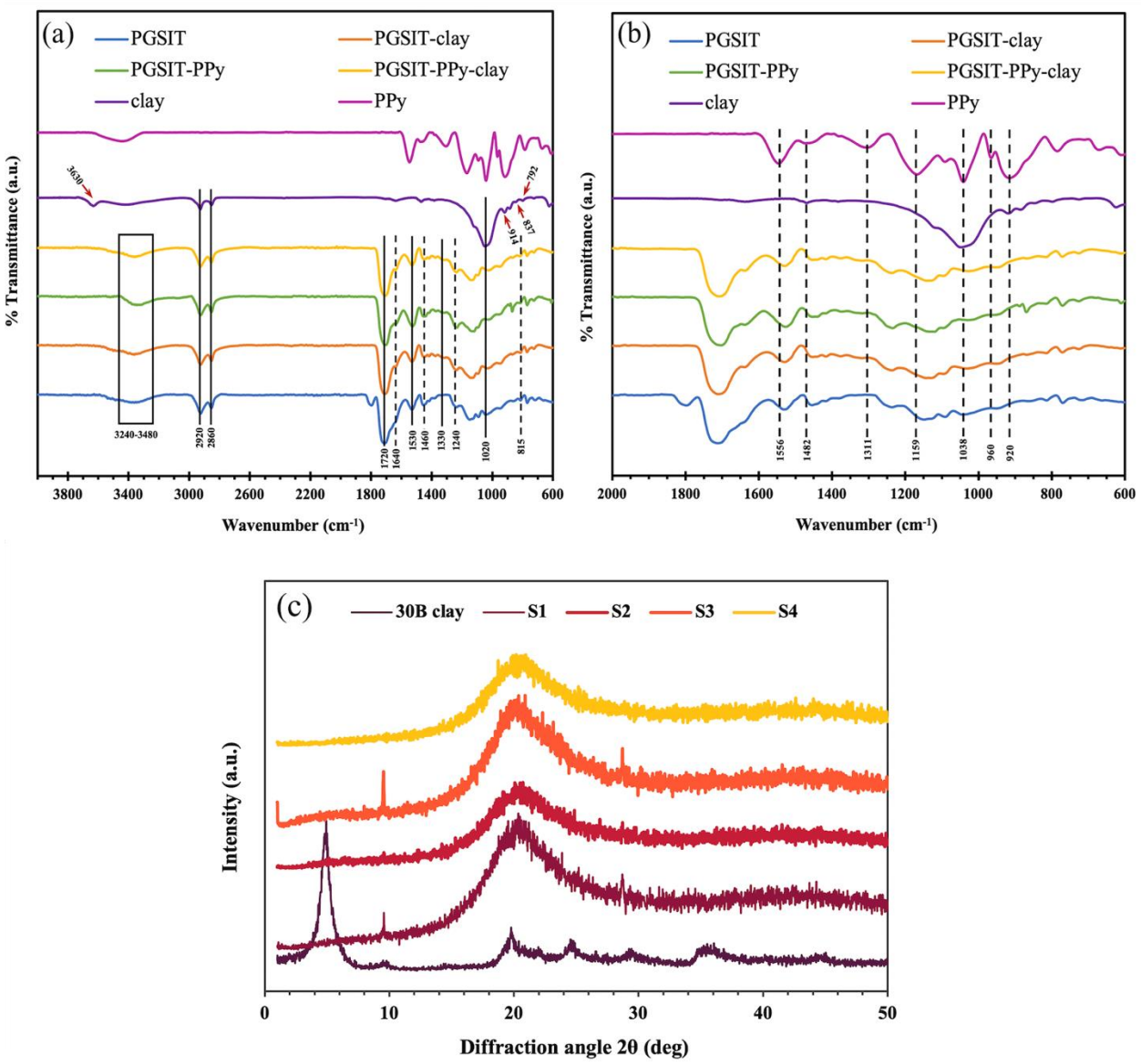

Fig.2 (a): Infrared spectra of synthesized PGSIT composites, clay, and PPy from 600 to 4000 cm^{-1}, **(b):** View of the infrared spectra within 600–2000 cm^{-1} range, **(c):** X-ray diffraction pattern of the synthesized biomaterials.

X-ray analysis was accomplished to evaluate the extent of clay dispersion and study the reflection patterns of crosslinked polyesters. The existence of a flattened peak around 2θ=20° confirmed the amorphous state of the prepared composite films (Fig.2c) [46]. This amorphous behavior in pure PGSIT is composed of the short-range ordered arrangement of cured chains and the disordered structure of the amorphous region within the matrix. The relative amorphous peak's

intensity at 2θ=20° dropped as PPy was blended with the system. The ordered microstructural regions of the matrix were affected by interfacial interactions of PPy with PGSIT as PPy could act as an impurity to disturb the ordered arrangement of the chains [14].

The well-characteristic diffraction peak of the clay particles (d_{001} value) was observed at 2θ=5° and the relative d-spacing of 1.76 nm was obtained according to the Bragg's formula ($n\lambda = 2d\sin\theta$). However, the XRD spectra of clay-contained samples showed no reflection corresponding to clay galleries, which may be due to the well-dispersion of exfoliated clay within the matrix [14].

3.2. Morphological visualization

The cross-section microstructure of the fabricated composites was studied by FE-SEM to detect the clay distribution in the PGSIT matrix. Fig.3 illustrates the FE-SEM micrograph images of the PGSIT-clay and PGSIT-PPy-clay samples. As is seen, the silicate platelets related to the clay were homogeneously distributed in PGSIT (Fig.3B1-2) and PGSIT-PPy (Fig.3A1-2) matrix. According to the homogeneous distribution, it can be related to the hydrogen connections involving the amine groups of PPy and hydroxyl groups in 30B clay and PGSIT. Moreover, as depicted in Fig.3A3-B3, the insertion of PSGIT chains into the clay galleries' spacing led to the formation of intercalated layered silicate structures and aided in the expansion and dispersion of clay within the polymer substrate.

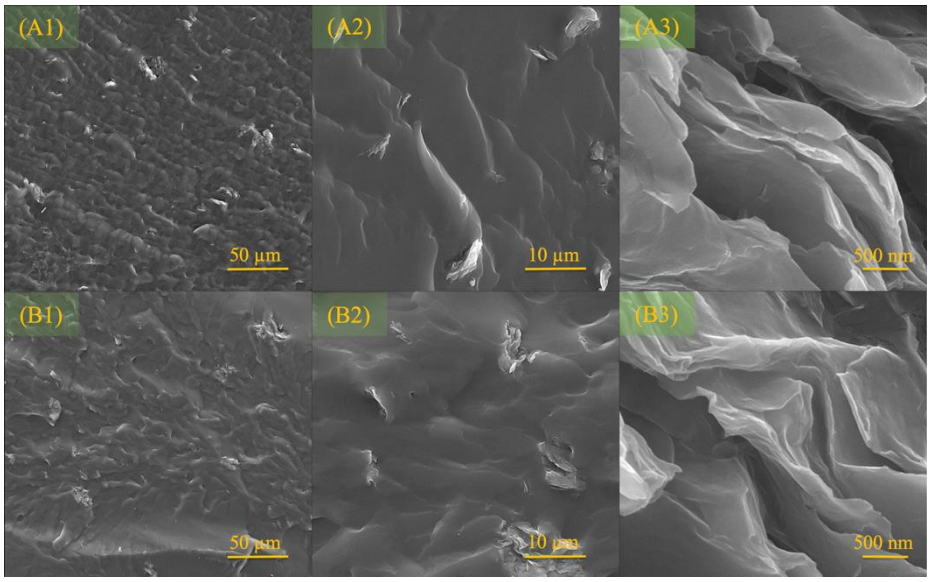

Fig.3: FE-SEM micrographs correspond to PGSIT-PPy-clay (A1-3), and PGSIT-clay (B1-3) with various magnification: (A1-B1) 1000X (50 μm), (A2-B2) 5000X (10 μm), and (A3-B3) 75000X (500 nm).

EDX-point analysis revealed the spatial distribution of PPy and clay within the PGSIT matrix. As shown in Fig.4, the minimum phase separation of nitrogen atoms related to PPy has been observed. The uniform dispersion of PPy through the matrix might be due to the strong hydrogen-bonding interactions among the PGSIT and PPy, which could facilitate the electrical conductivity of the composite [30]. As anticipated, carbon (C-blue dots) was the major element throughout the matrix as it was the major constituent element of both polymers (Table 2). Furthermore, silicon (Si-red dots) was selected to provide direct confirmation of the presence of clay particles in the composite. The pulled-out arrangement of the clay from the PGSIT-PPy matrix showed that the chemical interaction between the matrix and clay leads to strong adhesion between components. Based on the micrograph of Si mapping, it could also be inferred that along with the random distribution of layered silicate, some micro-clusters of Si related to clay aggregates were also formed within the biopolymer matrix. According to the absence of clay peaks in the XRD pattern and the existence of some macroaggregates in the matrix, it could be deduced that a broad mixture of heterogeneous microstructures ranging from single layers to intercalated galleries with random dispersion is present, and the XRD analysis does not demonstrate the whole microstructure of the composite [47].

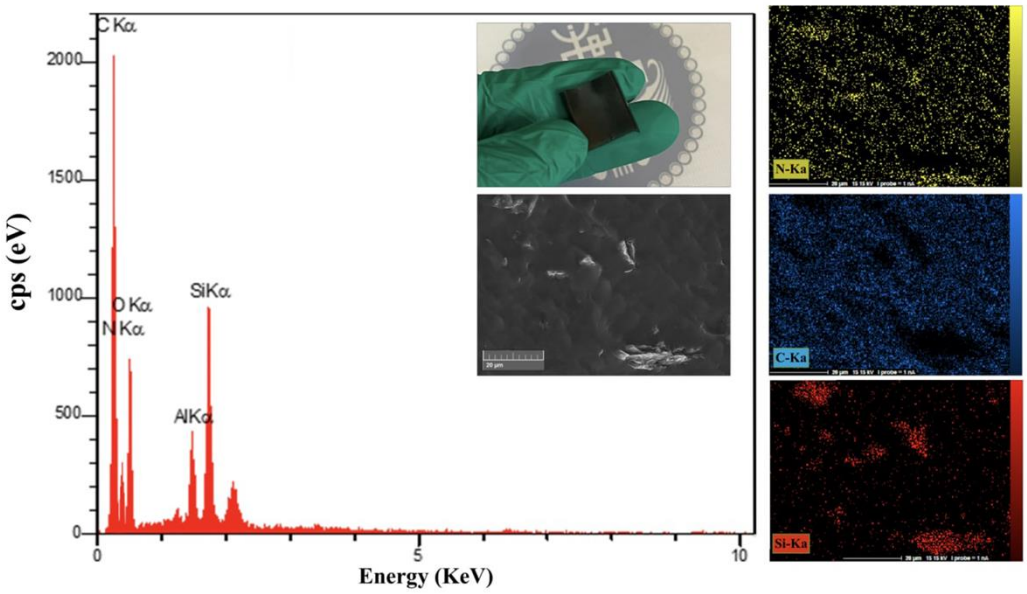

Fig.4: FE-SEM micrograph of PGSIT-PPy-clay composite and its corresponding EDX spectroscopy.

Table 2: The elemental composition of PGSIT-PPy-clay composite

Elt	C	N	O	Al	Si
W.%	47.94	23.43	21.64	2.82	4.16

3.3. Surface Wettability

The surface hydration behavior of the synthesized composite was evaluated using dynamic contact angle measurements. For each sample, the alteration of water contact angle (WCA) over time was depicted, as displayed in Fig.5 and listed in Table 3. Bypassing the assay's time, the angle of water with the samples' surface decreased, which shows their hydrophilicity (all samples had an initial WCA of less than 90°). Although PPy and clay could increase the hydrophilicity of PGSIT either when they were added separately or together, the WCA composite of PGSIT-PPy-clay was the lowest (60.8°).

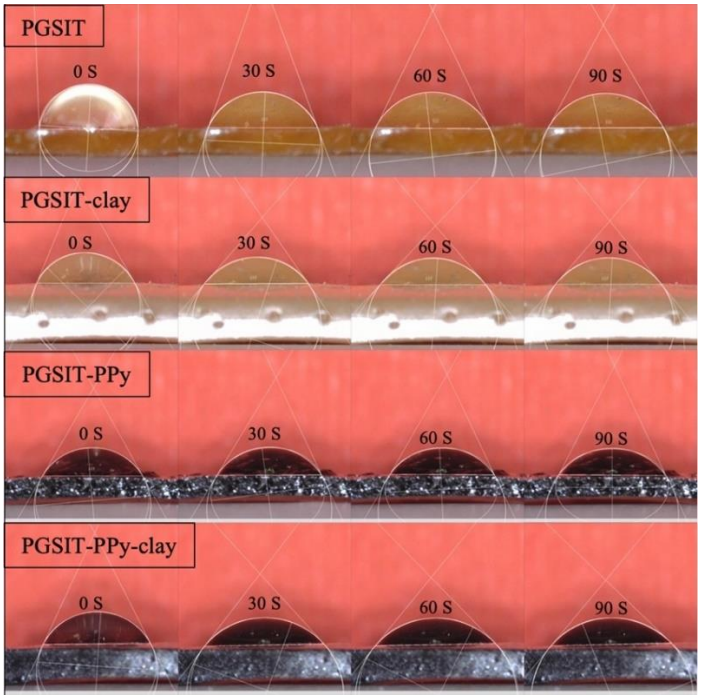

Fig.5: Graphical representation of samples and their WCA at various intervals (0, 30, 60, and 90 s).

Similar to other studies, the results confirmed the improvement of wettability as a consequence of the addition of clay and PPy [16,48]. This could be ascribed to the hydrophilic functional groups in the PPy (amine group) and clay (hydroxyl group) chemical structure [36,49]. These hydrophilic groups have a high attraction for polar water molecules due to the likelihood of hydrogen bonding interactions. The produced composites' hydrophilic nature can provide a moist environment that supports cell growth and adhesion [50].

Table 3: The data collected from WCA measurements at multiple wetting periods.

Time		0 s	30 s	60 s	90 s
Sample WCA at the varied wetting intervals (°)	PGSIT	91.4	70.4	64.2	60.8
	PGSIT-clay	63.8	52.2	50.2	47.9
	PGSIT-PPy	64.2	50.2	63.5	48.2
	PGSIT-PPy-clay	60.8	47.9	62	46

3.4. Electrical properties

The primary feature that a biomaterial should provide for substituting for electroactive tissue like nerve and cardiac is conductivity to the direct transmission of intercellular electrical signals. The conductivity of synthesized composites was determined using the four-point probe technique. In line with previous findings [30,35], the PPy-coated composite displayed a conductivity value of 1.04×10^{-4} S/cm, higher than its insulating counterpart (PGSIT: 5.9×10^{-11} S/cm). The results proved that the generation of hydrogen bonding interactions among the functional sites of PGSIT and PPy resulted in the homogeneous dispersion of PPy, by which an effective pathway of conductive PPy chains was built during the blending process. Moreover, the prepared materials were subjected to a closed-circuit assay to analyze their conductivity further. As illustrated in Fig.6, the pure PGSIT did not illuminate the LED bulb due to the insulating nature of PGSIT. However, the formation of conductive interconnected pathways of PPy throughout the PGSIT-PPy-clay composite led to the higher light output of the LED bulb.

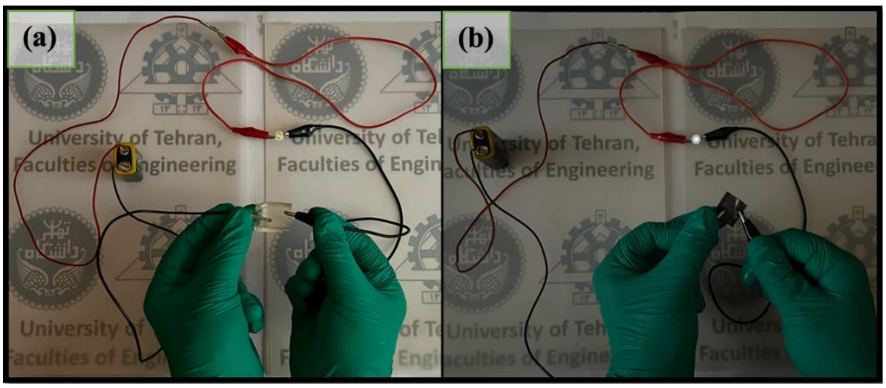

Fig.6: Images of (a) PPy-contained, and (B) pristine PGSIT films in a closed circuit experiment to evaluate their illumination capability with an LED.

3.5. Thermal stability

The influence of the clay and PPy on the thermal stability of PGSIT was analyzed via the TGA technique. The temperature-dependent profile of mass loss with the derivative curve (DTG) of the synthesized samples is illustrated in Fig.7. During the synthesis of PGSIT and its composites, the PGSIT pre-polymer was directly crosslinked with HDI by forming urethane linkages as described in FTIR section. Therefore, the two-step decomposition pattern of urethane-based compounds was found in the TGA curves of the samples [51]. The first step started around 220 °C and continued with the maximum rate of weight loss at 290 °C, which corresponded to the breakdown of urethane bonds [52]. The second step commenced at 350 °C and was followed by the maximum rate of weight loss at 425~445 °C, which was assigned to the chain dissociation of ester bonds [35,51,52]. Besides, the final decomposition stage emerged above 480 °C with an onset temperature of 539~553°C, which could be ascribed to the dehydrogenation and creation of advanced chain fragmentation as a consequence of the first and second decomposition steps, as well as the degradation of ashes produced in prior stages [35].

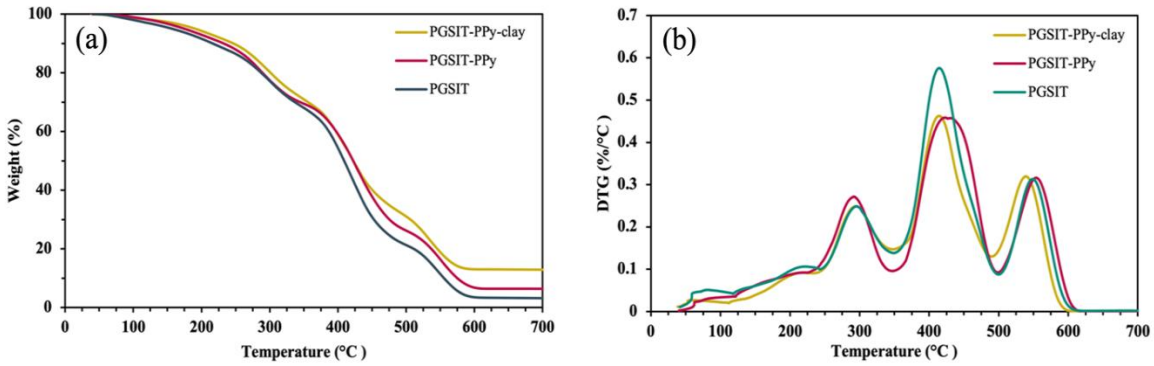

Fig.7: TGA (a) and DTG (b) graphs of the PGSIT-based samples.

The rigid π-conjugated molecular structure of PPy makes it a more thermally stable component and enables it to serve as a protective thermal barrier for the PGSIT substrate. Similar findings were reported for PPy-blended Poly (glycerol sebacate), in which the PPy retarded the decomposition profile [30]. In addition to PPy, incorporating clay increased the thermal stability of PGSIT. As demonstrated in the XRD section, PGSIT and clay have a strong interaction with each other due to their functional groups. Therefore, clay could act as a physical crosslinker and hinder the thermal decomposition of the matrix. Also, the dispersive morphology of clay illustrated in the FE-SEM section supplies a significant barrier effect in inhibiting the releasement of degraded components [14]. Finally, the samples' char residue was determined at 700 °C (Table 4). Compared to PGSIT with a char amount of 3.2%, adding PPy and clay-PPy increased the char value to 6.4% and 12.9%, respectively. The obtained char values confirmed that the hydrogen bonding interaction among each component resulted in the formation of interconnected crosslinked networks that remain stable in this temperature range.

Table 4: Thermometric data derived from TGA thermograms of the specimens.

Sample	T_{onset} (°C)	T_{10} (°C)	T_{50} (°C)	T_{Max1} (°C)	T_{Max2} (°C)	R_{700} (wt.%)
PGSIT	157	216	409	296	414	3.2
PGSIT-PPy	175	232	422	292	430	6.4
PGSIT-PPy-clay	190	246	422	295	414	12.9

Note: Tonset, T10, and T50 refer to the temperature at which the 5, 10, and 50% of weight loss eventuate. The temperatures that correspond to the highest rate of weight loss during

the initial and secondary steps of disintegration are regarded as T_{max1} and T_{max2}. R700 is the proportion of char that remained at 700°C.

3.6. Mechanical and viscoelastic properties

The mechanical compatibility of the composites with native tissues is essential as these materials need to supply desirable deformations to mimic the mechanical dynamics in host tissues [53]. Additionally, the mechanical characteristics of scaffolds can have a significant role in cell activities such as signaling, adhesion, and also cell growth [16]. The synthesized composite (PGSIT) demonstrated that in a hydrated condition (soaking in PBS solution at 37 ˚C for 48 h), they could withstand extreme deformation (bending) without breaking and cracking (Fig.8a-d). The hydrated biofilms were subjected to the tensile test, and their mechanical behavior and the summary of the collected data are represented in Fig.8 and Table 5.

As depicted in Fig.8b, all samples exhibited an almost linear elastic behavior. The neat PGSIT featured Young's modulus (Y.M.), ultimate tensile strength (UTS), and elongation at break (El) of 0.19 ± 0.015 MPa, 0.25 ± 0.02 MPa, and 123 ± 4%, which are in the range of soft tissues like skin, cornea, and human bladder [53]. It was detected that adding clay (3 wt.%) increased the Y.M. and UTS of the composite to 0.68 ± 0.13 MPa and 0.82 ± 0.03 MPa, respectively. It could be deduced that the uniform dispersion of clay in the matrix and the formation of strong interfacial interaction between polymer chains and filler particles provide the possibility for enhancement of the mechanical properties of the composite [54,55]. Also, compared with neat PGSIT, a slight decrease in El value was observed in the PGSIT-clay composite (El: 114.76 ± 1.52%). The reason for such a reduction might be related to the restriction effect of filler-polymer interactions on the polymer chains' movement and flexibility [55].

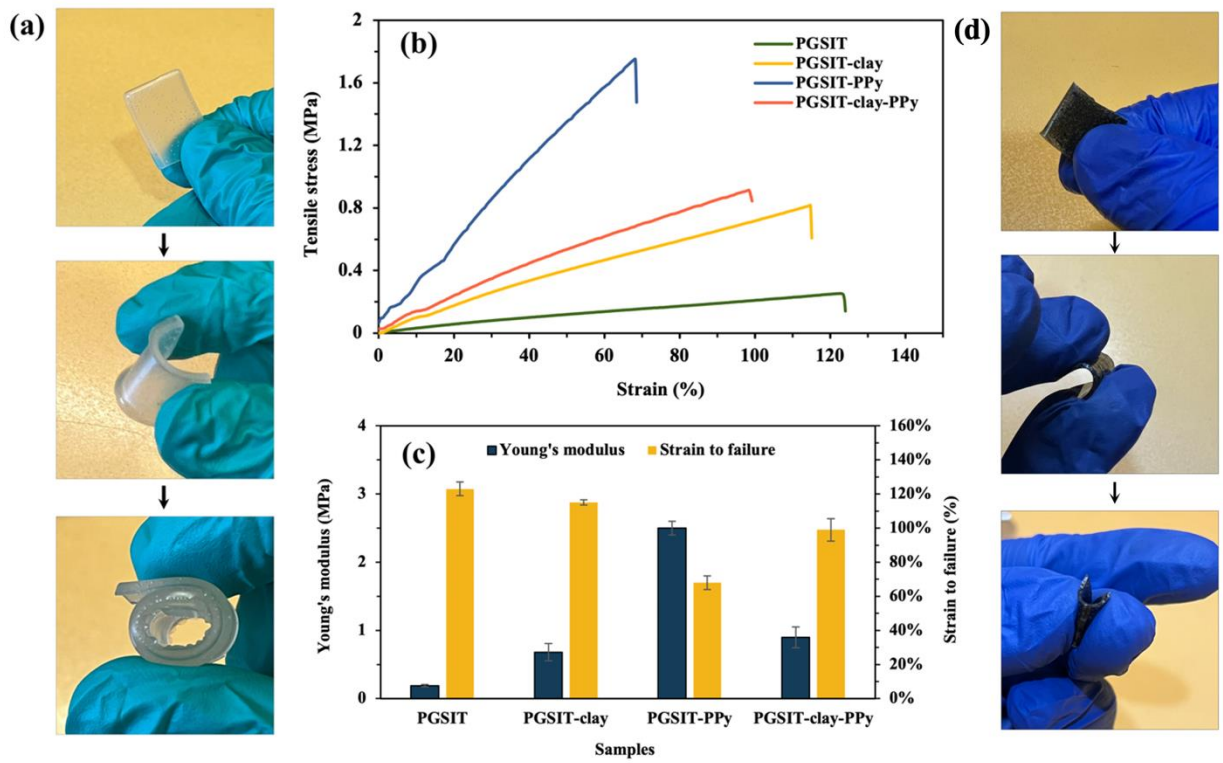

Fig.8: Tensile results of the prepared samples. (a) Demonstration of PGSIT and (d) PGSIT-PPy-clay feasibility in enduring intensive deformations without inducing any cracks or disintegrations. (b) The indicative strain-stress curves of PGSIT and its composite. (c) The obtained values of Young's modulus and strain to failure for each test sample.

On the other hand, the incorporation of PPy caused the increment in Y.M. and UTS of the PGSIT-PPy and reached the values of 2.5 ± 0.11 MPa and 1.75 ± 0.09 MPa, respectively (Fig.8c). It could also be seen that the blending of PPy strengthened the resultant composite and reduced the El value (El: 68.18 ± 4.31%). According to the literature [56], despite the desired electrical characteristics of PPy, this polymer is intrinsically brittle and has poor processability, which limits its application as a scaffold for tissue restoration. Hence, it could be inferred that the blending of PPy with elastic polymers like PGSIT increases the stiffness, although it makes the final scaffold more brittle. However, in the case of PGSIT with both clay and PPy components, the elastic behavior was better than in the PGSIT-PPy sample. The possible explanation could be attributed to the high aspect ratio of clay, which can exert strong interfacial interactions between polymer

and particles. Clay could act as a compatibilizer to create a strong interfacial zone between the hard (PPy) and soft (PGSIT) segments of the matrix. This interfacial zone between polymer matrix and clay can absorb tensile load from the brittle phase (PPy) and transfer it to the elastic phase (PGSIT). In addition, the similar polarity between the 30B modifier in clay and PPy segments in the matrix could improve the PPy dispersion in the PGSIT matrix during the blending process. Altogether, our findings demonstrated that PPy's shortcomings, such as poor processability, can be solved by combining it with elastic PGSIT containing clay.

Table 5: The collected data from strain-stress curves of fabricated biomaterials.

Sample	UTS (MPa)	El. (%)	Y.M. (MPa)
PGSIT	0.25±0.02	123.54±4.12	0.19±0.015
PGSIT-clay	0.82±0.03	114.76±1.52	0.68±0.13
PGSIT-PPy	1.75±0.09	68.18±4.31	2.5±0.11
PGSIT-PPy-clay	0.91±0.06	98.53±6.55	0.9±0.15

3.7. Biocompatibility

Biocompatibility is required for a substance to be classified as a biomaterial. In the present study, PGSIT and the composites based on PGSIT were synthesized using reactive monomers, which have been introduced as biocompatible and non-toxic materials [16,32,57–59]. To investigate the biocompatibility of the synthesized composites, the toxicity of the extracted media of the developed composites was evaluated by MTT assay.

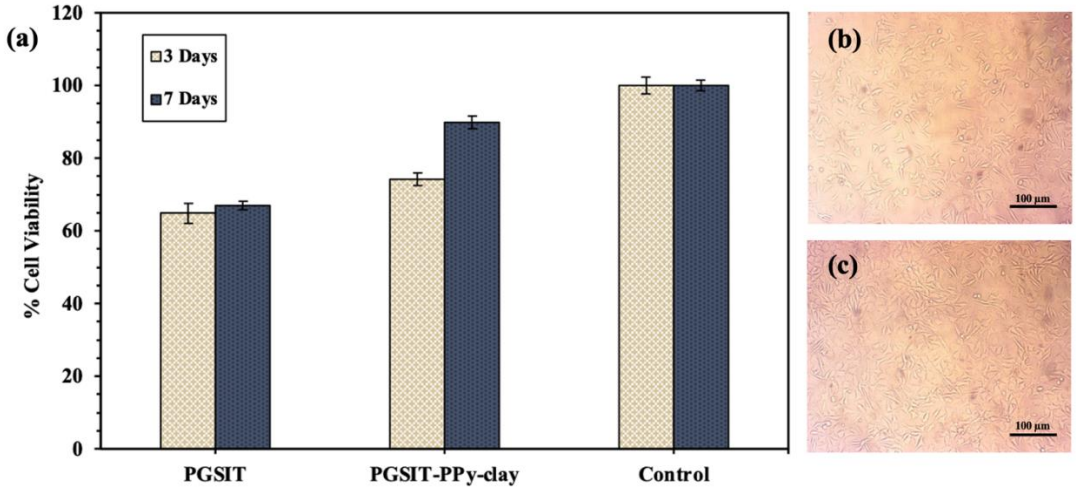

Fig.9 (a): The cell viability of the extracted media from PGSIT and PGSIT-PPy-clay after days three and seven, and the optical microscopic images of the morphology of the seeded cell in the extracted medium from **(b)** PGSIT and **(c)** PGSIT-PPy-clay after 7 days.

The viability of the L929 cells in the extracted media after three and seven days from the extraction was determined using MTT assays (Fig.9a). According to the MTT results, the PGSIT-PPy-clay composite showed acceptable biocompatibility since the cell viability more than 60% is an indicator for non-toxic materials. As is seen, the PGSIT-PPy-clay composite showed 8% and 22% higher cell viability than the PGSIT composite on days three and seven, respectively which might be due to the presence of PPy and clay in the extracted media[60]. Furthermore, the morphology of the cultured cells in the extracted media was investigated by an optical microscope (Fig.9b and c). The number of cells in the extracted medium from the PGSIT-PPy-clay was more than the cell number in the PGSIT extracted media.

The morphology of the cells on PGSIT-PPy-clay composite and PGSIT after seven days from cell culture were studied, which are shown in Fig.10. Compared to neat PGSIT (Fig.10a1), more cell spreading zones on the composite surface was detected after combining clay and PPy with PGSIT (Fig.10a2), which confirm the results of the cell viability assay. This better cell viability of PGSIT-PPy-clay composite than PGSIT might be due to the presence of PPy and clay as their positive effect on biocompatibility and cell metabolic activity has been proven[14].

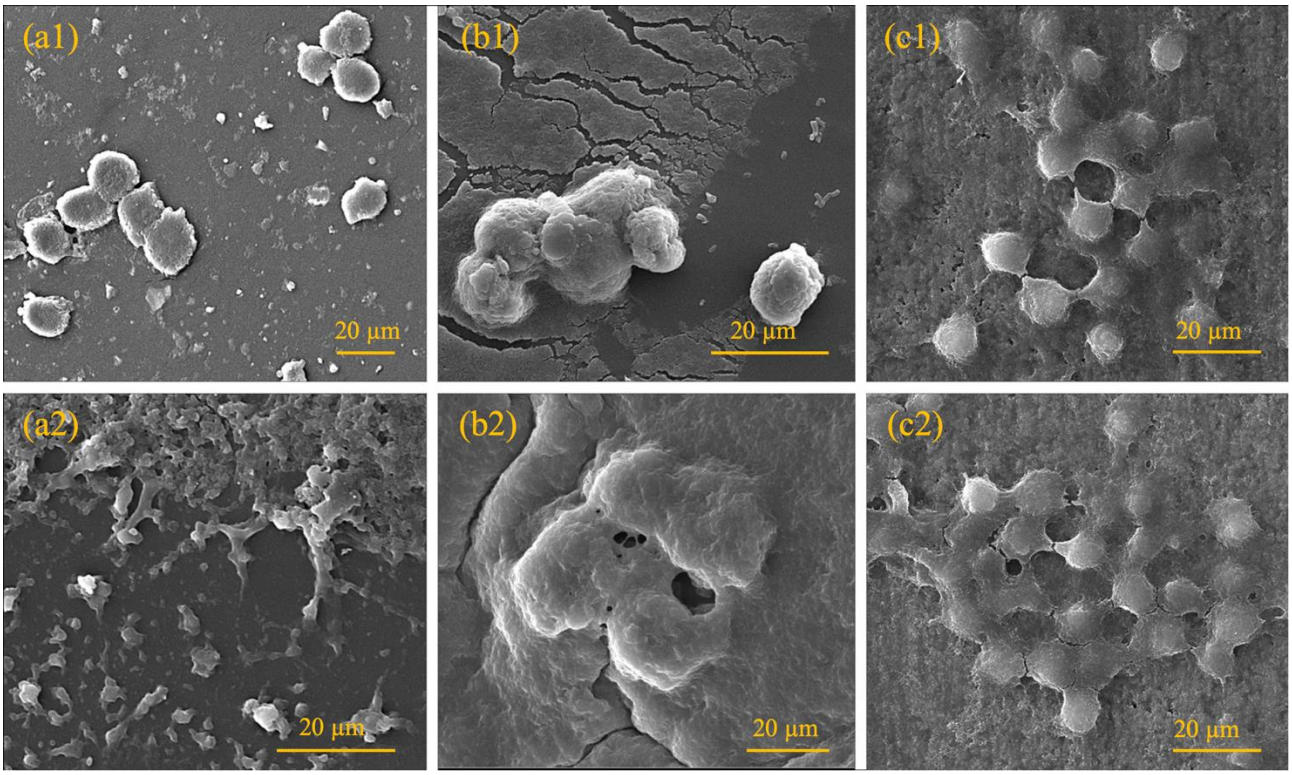

Fig.10 (a): SEM images of the morphology of L929 cells on the surface of (a1, b1, c1) PGSIT and (a2, b2. c2) PGSIT-PPy-clay after (a1-a2) 1, (b1-b2) 3, and (c1-c2) 7 days of cell incubation.

4. Conclusion

A reinforced conductive composite based on PGSIT, PPy, and clay was synthesized using a solvent-free approach, and the success of the synthesis was proven by comparing functional groups peaks of initial chemicals and PGSIT-PPy-clay. Due to the high interaction (hydrogen bonding) between amide groups of PPy with carbonyl, hydroxyl, and ester groups of PGSIT, PPy had a homogeneous dispersity within the PGSIT matrix, which was illustrated by XRD, SEM micrographs, and elemental mapping. Moreover, the intercalated layered silicate structure of the clay in a polymer substrate was further detected by FE-SEM images and EDX mapping. PGSIT-PPy-clay composite showed electrical conductivity values of 1.04×10^{-4} S/cm, which confirmed the continuous formation of conductive routes within the matrix. It was determined from the contact angle measurements that both PPy and clay enhanced the hydrophilicity of the PGSIT-PPy-clay composite due to their hydrophilic functional groups. The rigid molecular structure of

PPy and the thermophysical barrier properties of clay contributed to an improvement in composite thermal resistance and mechanical performance. Based on MTT analysis and morphology of cultured L929 cells, the PGSIT-PPy-clay composite had better cell viability than PGSIT. This study suggests that the PGSIT-PPy-clay composite can be tested in further development for soft tissue restoration.

Data availability

The raw/processed data required to reproduce these findings are available on request from the corresponding author. The data are not publicly available at this time as the data also forms part of an ongoing study.

Conflict of interest: Authors declare no conflict of interest

Acknowledgments : The authors wish to thank Hooman Golbaten-Mofrad, Morteza Mehrjoo and the other annotators involved in this paper, without whom this research would not have been possible. Our thanks also go to the reviewers for their considered feedback on our research.

References

[1] A. Arun, P. Malrautu, A. Laha, S. Ramakrishna, Gelatin Nanofibers in Drug Delivery Systems and Tissue Engineering, Eng. Sci. 16 (2021) 71–81. https://doi.org/10.30919/es8d527.

[2] S. Basak, Redesigning the modern applied medical sciences and engineering with shape memory polymers, Adv. Compos. Hybrid Mater. 4 (2021) 223–234. https://doi.org/10.1007/s42114-021-00216-1.

[3] R. Verma, A.B. Khan, A.K. Amar, M.I.K. Khan, S. Sah, Opto-structural Characteristics and Biomedical Applications of Microwave Irradiated Green Synthesised AM-AgNP from Atalantia monophylla (L.) Leaf Extract, ES Energy Environ. 17 (2022) 44–55. https://doi.org/10.30919/esee8c745.

[4] S. Ghosh, S. Ghosh, N. Pramanik, Bio-evaluation of doxorubicin (DOX)-incorporated hydroxyapatite (HAp)-chitosan (CS) nanocomposite triggered on osteosarcoma cells, Adv.

Compos. Hybrid Mater. 3 (2020) 303–314. https://doi.org/10.1007/s42114-020-00154-4.

[5] S. Vyas, A. Shukla, S.J. Shivhare, B. Vivekanand, N. Upadhyay, High Performance Conducting Nanocomposites Polyaniline (PANI)-CuO with Enhanced Antimicrobial Activity for Biomedical Applications, ES Mater. Manuf. 15 (2022) 46–52. https://doi.org/10.30919/esmm5f468.

[6] I. Armentano, M. Gigli, F. Morena, C. Argentati, L. Torre, S. Martino, Recent advances in nanocomposites based on aliphatic polyesters: Design, synthesis, and applications in regenerative medicine, Appl. Sci. 8 (2018). https://doi.org/10.3390/app8091452.

[7] Q. Chen, S. Liang, G.A. Thouas, Elastomeric biomaterials for tissue engineering, Prog. Polym. Sci. 38 (2013) 584–671. https://doi.org/10.1016/j.progpolymsci.2012.05.003.

[8] P. Ghaffari-Bohlouli, M. Shahrousvand, P. Zahedi, Performance evaluation of poly (L-lactide-co-D, L-lactide)/poly (acrylic acid) blends and their nanofibers for tissue engineering applications, Int. J. Biol. Macromol. 122 (2019) 1008–1016. https://doi.org/10.1016/j.ijbiomac.2018.09.046.

[9] P. Ghaffari-Bohlouli, F. Hamidzadeh, P. Zahedi, M. Shahrousvand, M. Fallah-Darrehchi, Antibacterial nanofibers based on poly(l-lactide-co-d, l-lactide) and poly(vinyl alcohol) used in wound dressings potentially: a comparison between hybrid and blend properties, J. Biomater. Sci. Polym. Ed. 31 (2020) 219–243. https://doi.org/10.1080/09205063.2019.1683265.

[10] P. Ghaffari-Bohlouli, H. Jafari, A. Khatibi, M. Bakhtiari, B. Tavana, P. Zahedi, A. Shavandi, Osteogenesis enhancement using poly (L-lactide-co-D, L-lactide)/poly (vinyl alcohol) nanofibrous scaffolds reinforced by phospho-calcified cellulose nanowhiskers, Int. J. Biol. Macromol. 182 (2021) 168–178. https://doi.org/10.1016/j.ijbiomac.2021.04.029.

[11] M. Abrisham, M. Noroozi, M. Panahi-Sarmad, M. Arjmand, V. Goodarzi, Y. Shakeri, H. Golbaten-Mofrad, P. Dehghan, A. Seyfi Sahzabi, M. Sadri, L. Uzun, The role of polycaprolactone-triol (PCL-T) in biomedical applications: A state-of-the-art review, Eur. Polym. J. 131 (2020). https://doi.org/10.1016/j.eurpolymj.2020.109701.

[12] P.K. Samantaray, A. Little, D.M. Haddleton, T. McNally, B. Tan, Z. Sun, W. Huang, Y. Ji, C. Wan, Poly(glycolic acid) (PGA): A versatile building block expanding high performance and sustainable bioplastic applications, Green Chem. 22 (2020) 4055–4081.

https://doi.org/10.1039/d0gc01394c.

[13] Q. Dasgupta, K. Chatterjee, G. Madras, Combinatorial approach to develop tailored biodegradable poly(xylitol dicarboxylate) polyesters, Biomacromolecules. 15 (2014) 4302–4313. https://doi.org/10.1021/bm5013025.

[14] H. Golbaten-mofrad, M. Hadi, S. Seyed, H. Jafari, V. Goodarzi, M. Entezari, M. Hashemi, Preparation and properties investigation of biodegradable poly (glycerol sebacate- co - gelatin) containing nanoclay and graphene oxide for soft tissue engineering applications, J. Biomed. Mater. Res. Part B Appl. Biomater. (2022) 1–17. https://doi.org/10.1002/jbm.b.35073.

[15] M. Asgharnejad-laskoukalayeh, H. Golbaten-Mofrad, S.H. Jafari, S. Seyfikar, P.Y. Talouki, A. Jafari, V. Goodarzi, S. Zamanlui, Preparation and Characterization of a New Sustainable Bio-Based Elastomer Nanocomposites Containing Poly (glycerol sebacate citrate)/Chitosan/n-Hydroxyapatite for Promising Tissue Engineering Applications, J. Biomater. Sci. Polym. Ed. 0 (2022) 1–18. https://doi.org/10.1080/09205063.2022.2104600.

[16] A. Jafari, V. Fakhri, S. Kamrani, S. Reza Ghaffarian Anbaran, C.H. Su, V. Goodarzi, V. Pirouzfar, H. Ali Khonakdar, Developemt of Flexible Nanocomposites Based on Poly(ε-caprolactone) for Tissue Engineering Application: The Contributing Role of Poly(glycerol succinic acid) and Polypyrrol, Eur. Polym. J. 164 (2022) 110984. https://doi.org/10.1016/j.eurpolymj.2021.110984.

[17] J. Dai, S. Ma, Y. Wu, L. Han, L. Zhang, J. Zhu, X. Liu, Polyesters derived from itaconic acid for the properties and bio-based content enhancement of soybean oil-based thermosets, Green Chem. 17 (2015) 2383–2392. https://doi.org/10.1039/c4gc02057j.

[18] G.Z. Yin, J.L. Díaz Palencia, D.Y. Wang, Fully bio-based Poly (Glycerol-Itaconic acid) as supporter for PEG based form stable phase change materials, Compos. Commun. 27 (2021). https://doi.org/10.1016/j.coco.2021.100893.

[19] L. Tian, M.P. Prabhakaran, J. Hu, M. Chen, F. Besenbacher, S. Ramakrishna, Synergistic effect of topography, surface chemistry and conductivity of the electrospun nanofibrous scaffold on cellular response of PC12 cells, Colloids Surfaces B Biointerfaces. 145 (2016) 420–429. https://doi.org/10.1016/j.colsurfb.2016.05.032.

[20] T. Nezakati, A. Seifalian, A. Tan, A.M. Seifalian, Conductive Polymers: Opportunities

and Challenges in Biomedical Applications, Chem. Rev. 118 (2018) 6766–6843. https://doi.org/10.1021/acs.chemrev.6b00275.

[21] J. Guo, Z. Chen, Z.M. El-Bahy, H. Liu, H.M. Abo-Dief, W. Abdul, K.M. Abualnaja, A.K. Alanazi, P. Zhang, M. Huang, G. Hu, J. Zhu, Tunable negative dielectric properties of magnetic CoFe2O4/graphite-polypyrrole metacomposites, Adv. Compos. Hybrid Mater. 5 (2022) 899–906. https://doi.org/10.1007/s42114-022-00485-4.

[22] W. Xie, F. Yao, H. Gu, A. Du, Q. Lei, N. Naik, Z. Guo, Magnetoresistive and piezoresistive polyaniline nanoarrays in-situ polymerized surrounding magnetic graphene aerogel, Adv. Compos. Hybrid Mater. 5 (2022) 1003–1016. https://doi.org/10.1007/s42114-021-00413-y.

[23] G. Li, L. Wang, X. Lei, Z. Peng, T. Wan, S. Maganti, M. Huang, V. Murugadoss, I. Seok, Q. Jiang, D. Cui, A. Alhadhrami, M.M. Ibrahim, H. Wei, Flexible, yet robust polyaniline coated foamed polylactic acid composite electrodes for high-performance supercapacitors, Adv. Compos. Hybrid Mater. 5 (2022) 853–863. https://doi.org/10.1007/s42114-022-00501-7.

[24] S. ur Rehman, R. Ahmed, K. Ma, S. Xu, T. Tao, M.A. Aslam, M. Amir, J. Wang, Composite of Strip-shaped ZIF-67 with Polypyrrole: A Conductive Polymer-MOF Electrode System for Stable and High Specific Capacitance, Eng. Sci. 13 (2021) 71–78. https://doi.org/10.30919/es8d1263.

[25] X. Xu, F. Yao, O.A.A. Ali, W. Xie, S.F. Mahmoud, P. Xie, S.M. El-Bahy, M. Huang, C. Liu, R. Fan, Z. Guo, A. Du, D. Estevez, F. Qin, H. Peng, D.P. Young, H. Gu, Adjustable core-sheath architecture of polyaniline-decorated hollow carbon nanofiber nanocomposites with negative permittivity for superb electromagnetic interference shielding, Adv. Compos. Hybrid Mater. 5 (2022) 2002–2011. https://doi.org/10.1007/s42114-022-00538-8.

[26] L. Ouyang, W. Huang, M. Huang, B. Qiu, Polyaniline improves granulation and stability of aerobic granular sludge, Adv. Compos. Hybrid Mater. 5 (2022) 1126–1136. https://doi.org/10.1007/s42114-022-00450-1.

[27] H. Li, W. Huang, B. Qiu, H.K. Thabet, D. Alhashmialameer, M. Huang, Z. Guo, Effective removal of proteins and polysaccharides from biotreated wastewater by polyaniline composites, Adv. Compos. Hybrid Mater. 5 (2022) 1888–1898.

https://doi.org/10.1007/s42114-022-00508-0.

[28] Y. Liang, J.C.-H. Goh, Polypyrrole-Incorporated Conducting Constructs for Tissue Engineering Applications: A Review, Bioelectricity. 2 (2020) 101–119. https://doi.org/10.1089/bioe.2020.0010.

[29] E. Fantino, I. Roppolo, D. Zhang, J. Xiao, A. Chiappone, M. Castellino, Q. Guo, C.F. Pirri, J. Yang, 3D Printing/Interfacial Polymerization Coupling for the Fabrication of Conductive Hydrogel, Macromol. Mater. Eng. 303 (2018) 1–8. https://doi.org/10.1002/mame.201700356.

[30] M.M. Sander, C.A. Ferreira, Synthesis and characterization of a conductive and self-healing composite, Synth. Met. 243 (2018) 58–66. https://doi.org/10.1016/j.synthmet.2018.06.003.

[31] N. Zanjanizadeh Ezazi, R. Ajdary, A. Correia, E. Mäkilä, J. Salonen, M. Kemell, J. Hirvonen, O.J. Rojas, H.J. Ruskoaho, H.A. Santos, Fabrication and Characterization of Drug-Loaded Conductive Poly(glycerol sebacate)/Nanoparticle-Based Composite Patch for Myocardial Infarction Applications, ACS Appl. Mater. Interfaces. 12 (2020) 6899–6909. https://doi.org/10.1021/acsami.9b21066.

[32] Y. Wang, G.A. Ameer, B.J. Sheppard, R. Langer, A tough biodegradable elastomer, Nat. Biotechnol. 20 (2002) 602–606. https://doi.org/10.1038/nbt0602-602.

[33] X.J. Loh, A. Abdul Karim, C. Owh, Poly(glycerol sebacate) biomaterial: synthesis and biomedical applications, J. Mater. Chem. B. 3 (2015) 7641–7652. https://doi.org/10.1039/c5tb01048a.

[34] R. Rai, M. Tallawi, A. Grigore, A.R. Boccaccini, Synthesis, properties and biomedical applications of poly(glycerol sebacate) (PGS): A review, Prog. Polym. Sci. 37 (2012) 1051–1078. https://doi.org/10.1016/j.progpolymsci.2012.02.001.

[35] H. Golbaten-Mofrad, A. Seyfi Sahzabi, S. Seyfikar, M.H. Salehi, V. Goodarzi, F.R. Wurm, S.H. Jafari, Facile template preparation of novel electroactive scaffold composed of polypyrrole-coated poly(glycerol-sebacate-urethane) for tissue engineering applications, Eur. Polym. J. 159 (2021) 110749. https://doi.org/10.1016/j.eurpolymj.2021.110749.

[36] S. Seyfikar, M. Asgharnejad-laskoukalayeh, S.H. Jafari, V. Goodarzi, M.H. Salehi, S. Zamanlui, Introducing a new approach to preparing bionanocomposite sponges based on

poly(glycerol sebacate urethane) (PGSU) with great interconnectivity and high hydrophilicity properties for application in tissue engineering, Eur. Polym. J. 173 (2022) 111239. https://doi.org/10.1016/J.EURPOLYMJ.2022.111239.

[37] M.H. Salehi, H. Golbaten-Mofrad, S.H. Jafari, V. Goodarzi, M. Entezari, M. Hashemi, S. Zamanlui, Electrically conductive biocompatible composite aerogel based on nanofibrillated template of bacterial cellulose/polyaniline/nano-clay, Int. J. Biol. Macromol. 173 (2021) 467–480. https://doi.org/10.1016/j.ijbiomac.2021.01.121.

[38] E. Alonso, M. Faria, F. Mohammadkazemi, M. Resnik, A. Ferreira, N. Cordeiro, Conductive bacterial cellulose-polyaniline blends: Influence of the matrix and synthesis conditions, Carbohydr. Polym. 183 (2018) 254–262. https://doi.org/10.1016/j.carbpol.2017.12.025.

[39] I.H. Jaafar, M.M. Ammar, S.S. Jedlicka, R.A. Pearson, J.P. Coulter, Spectroscopic evaluation, thermal, and thermomechanical characterization of poly(glycerol-sebacate) with variations in curing temperatures and durations, J. Mater. Sci. 45 (2010) 2525–2529. https://doi.org/10.1007/s10853-010-4259-0.

[40] T. Wu, M. Frydrych, K.O. Kelly, B. Chen, Poly(glycerol sebacate urethane)−Cellulose Nanocomposites with Water-Active Shape-Memory Effects, Biomacromolecules. 15 (2014) 2663–2671.

[41] M.J.N. Pereira, B. Ouyang, C.A. Sundback, N. Lang, I. Friehs, S. Mureli, I. Pomerantseva, J. McFadden, M.C. Mochel, O. Mwizerwa, P. Del Nido, D. Sarkar, P.T. Masiakos, R. Langer, L.S. Ferreira, J.M. Karp, A highly tunable biocompatible and multifunctional biodegradable elastomer, Adv. Mater. 25 (2013) 1209–1215. https://doi.org/10.1002/adma.201203824.

[42] S. Yu, J. Shi, Y. Liu, J. Si, Y. Yuan, C. Liu, A mechanically robust and flexible PEGylated poly(glycerol sebacate)/β-TCP nanoparticle composite membrane for guided bone regeneration, J. Mater. Chem. B. 7 (2019) 3279–3290. https://doi.org/10.1039/c9tb00417c.

[43] M.A. Chougule, S.G. Pawar, P.R. Godse, R.N. Mulik, S. Sen, V.B. Patil, Synthesis and Characterization of Polypyrrole (PPy) Thin Films, Soft Nanosci. Lett. 01 (2011) 6–10. https://doi.org/10.4236/snl.2011.11002.

[44] H. Eisazadeh, Studying the Characteristics of Polypyrrole and its Composites, World J.

Chem. 2 (2007) 67–74.

[45] S.S. Babu, N. Kalarikkal, S. Thomas, E.K. Radhakrishnan, Enhanced antimicrobial performance of cloisite 30B/poly (ε-caprolactone) over cloisite 30B/poly (L-lactic acid) as evidenced by structural features, Appl. Clay Sci. 153 (2018) 198–204. https://doi.org/10.1016/j.clay.2017.12.003.

[46] Q.Z. Chen, A. Bismarck, U. Hansen, S. Junaid, M.Q. Tran, S.E. Harding, N.N. Ali, A.R. Boccaccini, Characterisation of a soft elastomer poly(glycerol sebacate) designed to match the mechanical properties of myocardial tissue, Biomaterials. 29 (2008) 47–57. https://doi.org/10.1016/j.biomaterials.2007.09.010.

[47] S.K. Rath, K. Sudarshan, R.S. Bhavsar, U.K. Kharul, P.K. Pujari, M. Patri, D. V. Khakhar, Characterizing the nanoclay induced constrained amorphous region in model segmented polyurethane-urea/clay nanocomposites and its implications on gas barrier properties, Phys. Chem. Chem. Phys. 18 (2016) 1487–1499. https://doi.org/10.1039/c5cp05260b.

[48] B. Maharjan, V.K. Kaliannagounder, S.R. Jang, G.P. Awasthi, D.P. Bhattarai, G. Choukrani, C.H. Park, C.S. Kim, In-situ polymerized polypyrrole nanoparticles immobilized poly(ε-caprolactone) electrospun conductive scaffolds for bone tissue engineering, Mater. Sci. Eng. C. 114 (2020) 111056. https://doi.org/10.1016/j.msec.2020.111056.

[49] B. Sun, T. Wu, J. Wang, D. Li, J. Wang, Q. Gao, M.A. Bhutto, H. El-Hamshary, S.S. Al-Deyab, X. Mo, Polypyrrole-coated poly(L-lactic acid-co-e- caprolactone)/silk fibroin nanofibrous membranes promoting neural cell proliferation and differentiation with electrical stimulation, J. Mater. Chem. B. 4 (2016) 6670–6679. https://doi.org/10.1039/c6tb01710j.

[50] H.-I. Chang, Y. Wang, Cell Responses to Surface and Architecture of Tissue Engineering Scaffolds, Regen. Med. Tissue Eng. - Cells Biomater. (2011). https://doi.org/10.5772/21983.

[51] G. Trovati, E.A. Sanches, S.C. Neto, Y.P. Mascarenhas, G.O. Chierice, Characterization of polyurethane resins by FTIR, TGA, and XRD, J. Appl. Polym. Sci. 115 (2010) 263–268. https://doi.org/https://doi.org/10.1002/app.31096.

[52] B.R. Barrioni, S.M. De Carvalho, R.L. Oréfice, A.A.R. De Oliveira, M.D.M. Pereira,

Synthesis and characterization of biodegradable polyurethane films based on HDI with hydrolyzable crosslinked bonds and a homogeneous structure for biomedical applications, Mater. Sci. Eng. C. 52 (2015) 22–30. https://doi.org/10.1016/j.msec.2015.03.027.

[53] C.F. Guimarães, L. Gasperini, A.P. Marques, R.L. Reis, The stiffness of living tissues and its implications for tissue engineering, Nat. Rev. Mater. 5 (2020) 351–370. https://doi.org/10.1038/s41578-019-0169-1.

[54] X. Zhai, Y. Ma, C. Hou, F. Gao, Y. Zhang, C. Ruan, H. Pan, W.W. Lu, W. Liu, 3D-Printed High Strength Bioactive Supramolecular Polymer/Clay Nanocomposite Hydrogel Scaffold for Bone Regeneration, ACS Biomater. Sci. Eng. 3 (2017) 1109–1118. https://doi.org/10.1021/acsbiomaterials.7b00224.

[55] F. Zia, Z. i. H. Nazli, K.M. Zia, W. Aftab, S. Tabasum, M. Asrar, Synthesis and characterization of hydroxyethyl cellulose copolymer modified polyurethane bionanocomposites, Int. J. Biol. Macromol. 179 (2021) 345–352. https://doi.org/10.1016/j.ijbiomac.2021.03.029.

[56] Z. Zhang, M. Rouabhia, Z. Wang, C. Roberge, G. Shi, P. Roche, J. Li, L.H. Dao, Electrically conductive biodegradable polymer composite for nerve regeneration: Electricity-stimulated neurite outgrowth and axon regeneration, Artif. Organs. 31 (2007) 13–22. https://doi.org/10.1111/j.1525-1594.2007.00335.x.

[57] M. Mousa, N.D. Evans, R.O.C. Oreffo, J.I. Dawson, Clay nanoparticles for regenerative medicine and biomaterial design: A review of clay bioactivity, Biomaterials. 159 (2018) 204–214. https://doi.org/10.1016/j.biomaterials.2017.12.024.

[58] A.K. Gaharwar, L.M. Cross, C.W. Peak, K. Gold, J.K. Carrow, A. Brokesh, K.A. Singh, 2D Nanoclay for Biomedical Applications: Regenerative Medicine, Therapeutic Delivery, and Additive Manufacturing, Adv. Mater. 31 (2019) 1–28. https://doi.org/10.1002/adma.201900332.

[59] R. Prabakaran, J.M. Marie, A.J.M. Xavier, Biobased Unsaturated Polyesters Containing Castor Oil-Derived Ricinoleic Acid and Itaconic Acid: Synthesis, in Vitro Antibacterial, and Cytocompatibility Studies, ACS Appl. Bio Mater. 3 (2020) 5708–5721. https://doi.org/10.1021/acsabm.0c00480.

[60] E.N. Zare, T. Agarwal, A. Zarepour, F. Pinelli, A. Zarrabi, F. Rossi, M. Ashrafizadeh, A. Maleki, M.A. Shahbazi, T.K. Maiti, R.S. Varma, F.R. Tay, M.R. Hamblin, V. Mattoli, P.

Makvandi, Electroconductive multi-functional polypyrrole composites for biomedical applications, Appl. Mater. Today. 24 (2021) 101117. https://doi.org/10.1016/j.apmt.2021.101117.